# X-Ray Specular-Reflectivity Study of the Liquid-Vapor Density Profile of \(^4\)He

# X-ray specular-reflectivity study of the liquid-vapor density profile of $^4$He

L. B. Lurio*
*Department of Physics, Harvard University, Cambridge, Massachusetts 02138*

T. A. Rabedeau†
*Division of Applied Sciences, Harvard University, Cambridge, Massachusetts 02138*

P. S. Pershan
*Department of Physics, Harvard University, Cambridge, Massachusetts 02138*
*and Division of Applied Sciences, Harvard University, Cambridge, Massachusetts 02138*

Isaac F. Silvera
*Department of Physics, Harvard University, Cambridge, Massachusetts 02138*

M. Deutsch
*Physics Department, Bar Ilan University, Ramat Gan 52100, Israel*

S. D. Kosowsky
*Department of Physics, Harvard University, Cambridge, Massachusetts 02138*

B. M. Ocko
*Physics Department, Brookhaven National Laboratory, Upton, New York, 11973-5000*
(Received 4 January 1993; revised manuscript received 20 May 1993)

The helium liquid-vapor interfacial density profile has been measured with x-ray specular reflectivity. Measurements were performed on thick films of helium adsorbed onto atomically flat silicon substrates. Both the amplitude and the phase of the complex scattering amplitude of the helium-vapor interface were obtained from measured interference between reflections from the helium liquid-vapor interface and the silicon-helium interface. Films whose thickness varied from 15 Å to 220 Å over a range of temperatures from 1.1 K to 3.0 K were studied. At $T=1.13$ K the film thickness is 215 Å and the interfacial width is $9.2\pm1$ Å. No significant variation was seen in the interfacial widths measured at temperatures between 1.1 K and 1.8 K. Analysis of these measurements indicates that the interface is asymmetric, with the decay of the density into the vapor having the sharper falloff. The zero-K interfacial width extrapolated from the finite-temperature measurements with a quantized capillary-wave theory is $7.6^{+1}_{-2}$ Å.

## I. INTRODUCTION

In this paper we present our measurements and analysis of x-ray studies of the gradual transition in density at the interface between the liquid and vapor phases of helium. This system has been the subject of extensive studies addressing long-standing questions about the nature of an inhomogeneous Bose liquid,[1,2] as well as an important part of the larger search to understand the nature of the liquid surface in general.[3] Recent relevant experiments include reflection of atomic hydrogen[4] and helium[5] from the superfluid helium surface, measurements of the bound states of electrons,[6] the adsorption potential of atomic hydrogen[7] and $^3$He on the helium surface;[8] scattering of neutrons from helium films;[9] and experiments on the interaction of quantized excitations in bulk helium with the helium surface.[10,11] Concurrent theoretical progress has primarily resulted from analysis of the statistical mechanics of surface excitations,[12,13] computer simulations, and new density functional theories,[2,14–20] however, it was also stimulated by above-mentioned experimental results.[5,21] Although many of the experiments are sensitive to aspects of the liquid-vapor interface, recovering details of the helium interfacial profile from them is quite difficult. For example, information has been obtained from atomic scattering experiments[5] but the interpretation of these results is complicated by the nature of the interactions of the probe atoms with the liquid surface.

Ellipsometry measurements, such as were performed by Osborne,[22] employ visible light whose wavelength is long compared to the width of the interfaces, and consequently only obtain information that integrates over the surface profile. By contrast, x-ray specular reflectivity provides angstrom level resolution of the interfacial electron-density profile.[23] X-ray scattering from $^4$He is hampered by the small scattering cross section of the helium atom; however, by utilizing the combination of an intense synchrotron x-ray source and an interference scattering geometry, we have measured details of the

 

liquid-vapor interface of superfluid $^4$He with a resolution along the surface normal of $\sim 2$ Å. Some of these results have been previously published.[24,25]

In Sec. II we shall briefly review the basic aspects of specular reflectivity and describe the interference geometry that was used in the present experiment in order to increase the signal intensity and gain sensitivity to the asymmetry of the interfacial profile. In Secs. III and IV we shall present the experimental details and explain the method for relating the measured reflectivity to a specific model of the liquid-vapor interfacial profile. Finally, in Secs. V and VI we shall discuss the results of the experiment in the context of several current theoretical and experimental measurements.

## II. X-RAY REFLECTIVITY

### A. Introduction to specular reflectivity

With the advent of high intensity synchrotron sources x-ray specular reflectivity has become a well-established technique for measuring surface electron-density profiles.[26] In this method, deviations between the measured x-ray specular reflectivity $R(Q)$ for a real surface and the theoretical reflectivity from a perfectly sharp flat interface, $R_F(Q)$, given by Fresnel's law of optics are related to the density profile across the interface. It is convenient to express the ratio, $R(Q)/R_F(Q)$ in terms of a complex scattering amplitude $\Phi(Q)$

$$R(Q)/R_F(Q)=|\Phi(Q)|^2 , \tag{2.1}$$

where the magnitude of the wave-vector transfer is given by $Q=|\mathbf{Q}|=2K\sin\theta$, $\theta$ is the angle of incidence, and $K=|\mathbf{K}_{\rm inc}|=2\pi/\lambda$ is the wave vector of the incident light [see Fig. 1(a)]. For $\theta \gg \theta_c$, where $\theta_c$ is the critical angle below which x-rays are 100% reflected, $\Phi(Q)$ is very well approximated by

$$\Phi(Q)=\frac{1}{\rho_\infty}\int_{-\infty}^{\infty}\frac{d\langle\rho(z)\rangle_{x,y}}{dz}e^{iQz}dz . \tag{2.2}$$

Here $\langle\rho(z)\rangle_{x,y}$ is the electron density at depth $z$, averaged over the projection of the x-ray coherence area on the plane of the surface, and $\rho_\infty$ is the bulk electron density. For the present measurement the projected x-ray coherence length in the plane of incidence was typically of order 4000 Å. Further details of the resolution are discussed below. In addition, for $\theta$ approximately equal to $\theta_c$ this approximation for $\Phi(Q)$ is not accurate and, as discussed in Sec. IV A 4 below, the ratio of $R(Q)/R_F(Q)$ must be calculated using a procedure similar to that of Parrat.[27]

At large angles the Fresnel reflectivity $R_F$ falls off as $(Q_c/2Q)^4$ where

$$Q_c=\sqrt{16\pi\rho_\infty r_e}=(4\pi/\lambda)\sin(\theta_c)$$

corresponds to the wave-vector transfer at the critical angle for total external reflection, $\theta_c$, and $r_e$ is the classical electron radius. For liquid helium $Q_c=0.0077$ Å$^{-1}$. In view of the fact that the sensitivity to structural details of size $d$ requires measurements of $\Phi(Q)$ to wave-vector transfer of order $Q=1/d$, the rapid falloff of $R_F(Q)$ with increasing $Q$ limits the technique. For example, to probe details of the helium liquid-vapor interface of size $\sim 2$ Å requires measurements to $Q$ of order 0.5 Å$^{-1}$.[28] At this value of $Q$, $R_F(Q)$ for bulk helium has a value of $4\times10^{-9}$. As seen from Eq. (2.2), interface roughness or diffusiveness reduces the reflectivity further. In general, this feature eventually limits the range of any specular reflectivity measurement; however, in the present experiment the low value of the helium electron density makes this limitation particularly severe.

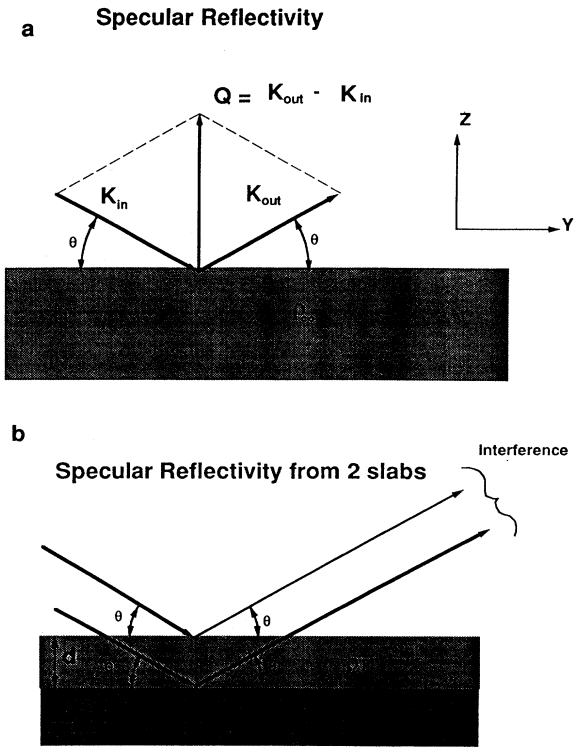


FIG. 1. (a) Reflectivity from a semi-infinite substrate. The vectors $\mathbf{K}_{\rm inc}$ and $\mathbf{K}_{\rm out}$ are the wave vectors of the incident and reflected x rays, respectively. (b) Interference reflection geometry.

### B. Interference method

The above-mentioned limitation to the reflectivity technique is partially circumvented by measuring the reflectivity from a thick ($\sim 200$ Å) film of liquid helium adsorbed onto a flat dense solid substrate. The reflectivity from such a composite surface [see Fig. 1(b)] can be given by $R_{12}=|E_{12}^R|^2$, where

$$E_{12}^R=\frac{E_2^R+E_1^R e^{iQd}}{1+E_1^R E_2^R e^{iQd}} . \tag{2.3}$$

Here, the thickness of the film is $d$, $E_{12}^R$ is the complex

amplitude for the reflected electric field given an incident monochromatic plane wave of unit amplitude, while $E_1^R$ and $E_2^R$ are the electric fields that would be reflected in isolation from the vapor-film and solid-film interfaces, respectively.[29] In the approximation of $Q \gg Q_c$, the $E_i^R$ ($i=1,2$) can be expressed in terms of the complex amplitudes $\Phi_i(Q)$,

$$E_i^R = \Phi_i(Q)\sqrt{R_F(Q)_i}, \quad i=1 \text{ or } 2 , \tag{2.4}$$

where $R_F(Q)_i$ is the reflectivity for an ideally planar, and infinitesimally sharp, interface between the two bulk materials. For $Q \gg Q_c$ we can write

$$\sqrt{R_F(Q)_1} \approx (4\pi\rho_1 r_e/Q^2)$$

and

$$\sqrt{R_F(Q)_2} \approx [4\pi(\rho_2-\rho_1)r_e/Q^2] ,$$

and since both reflectivities are much less than unity, the composite reflectivity from two interfaces can be simplified to

$$\begin{aligned} R_{12}/R_{F2} &= |A\Phi_1(Q)\exp(iQd)+B\Phi_2(Q)|^2 \\ &= A^2|\Phi_1(Q)|^2+B^2|\Phi_2(Q)|^2+2AB\cos[Qd+\phi_1(Q)-\phi_2(Q)]|\Phi_1(Q)||\Phi_2(Q)| , \end{aligned} \tag{2.5}$$

where $A=\rho_1/\rho_2$, $B=(\rho_2-\rho_1)/\rho_2$ with $\rho_{1,2}$ the densities of the film and substrate, respectively, and $\phi_{1,2}$ are the phases of the complex $\Phi_{1,2}(Q)$.

### C. Advantages

For a helium film adsorbed onto a silicon substrate, the first two terms in Eq. (2.5) represent the reflection of x rays from the liquid-vapor interface and the silicon-liquid interface, respectively (i.e., 1=He, 2=Si). Since

$$A^2=(\rho_{\mathrm{He}}/\rho_{\mathrm{Si}})^2 \approx (0.06)^2$$

and $B^2 \approx (0.94)^2$ the first term is negligible compared to the second. The term proportional to $2AB$, which results from interference between reflections from the top and bottom interfaces of the film, is $\sim 13\%$ of the second term with an oscillating amplitude proportional to $|\Phi_{\mathrm{He}}(Q)|$. Hence for the interference technique, there is an increase by a factor of $2B/A = 1.88/0.06 \approx 31$ in the part of the signal proportional to $\Phi_{\mathrm{He}}(Q)$ compared to the reflectivity from a surface of bulk $^4$He. In addition, the interference technique is also sensitive to the relative phase difference between the two complex scattering amplitudes, $\phi_{\mathrm{He}}(Q)-\phi_{\mathrm{Si}}(Q)$. This sensitivity to the phase of $\Phi(Q)$ provides information about the asymmetry of $d\langle\rho\rangle/dz$. For example, if $d\langle\rho\rangle/dz$ is an even function, the phase is always zero. Hence if the phase of the reflectivity from the Si substrate is known the asymmetry of the density profile of the helium interface can be determined from measurement of the phase difference $\phi_{\mathrm{He}}(Q)-\phi_{\mathrm{Si}}(Q)$.

### D. Limitations

The primary limitations of this technique are that the thickness of the film must be constant over the surface area illuminated by the x-ray beam, stable in time, and insensitive to the level of incident x-ray flux. In this study it was found that for unsaturated helium films below the lambda point the film thickness was indeed uniform, stable, and insensitive to x-ray flux. Hence the interference method could be applied for these films. As will be discussed below for saturated films sufficiently stable films were not obtained, while for films above the lambda point x-ray flux related problems prevented collection of data out to sufficiently large values of $Q$.

A further limitation is associated with the reflection from the silicon-helium interface. Because this reflection is more intense than the interference term by the same factor $\rho_{\mathrm{Si}}/\rho_{\mathrm{He}}$ that the interference term is stronger than the helium surface reflection, the statistical fluctuations in the amplitude of this signal will be much larger than the counting statistical noise from just the interference term alone. It follows that if counting statistics were the dominant noise source there would be no statistical advantage to using the interference method over a direct specular reflectivity measurement. However, counting statistics are not usually the limiting noise source. For example, if a specular reflectivity measurement were performed on a deep puddle of helium the background due to diffuse scattering from the bulk liquid would exceed the specular reflectivity for wave-vector transfer $Q > 0.5$ Å$^{-1}$.[30] By contrast in the present geometry, since the crystalline silicon has negligible diffuse scattering, scattering from the bulk is not important and the practical limit to the measurement of the specular reflectivity due to the other noise sources is $Q \approx 0.7$ Å$^{-1}$.

## III. EXPERIMENTAL DETAILS

The majority of the experimental measurements reported here were performed at beamline X22B of the National Synchrotron Light Source (NSLS) at Brookhaven National Laboratory; however, some initial results were obtained using the rotating anode source at the Harvard Materials Research Laboratory. The measurements were made using a horizontal two circle spectrometer configuration upon which a $^4$He cryostat capable of operating between 1.1 and 4.2 K was mounted concentric to the vertical $\Theta$-$2\Theta$ axis of the spectrometer.

Figure 2 depicts the cryostat, sample chamber, and the scattering geometry used at NSLS. The incident arm of the spectrometer (from the x-ray source to the sample), serves to monochromatize the x-ray beam, define the in-

cident resolution in the vertical and horizontal directions, remove background scattering from slit edges and air, and monitor the intensity of the incident x-ray beam. A doubly curved mirror was used to focus the beam to a small spot at the sample and a Ge(111) crystal was set to select $\lambda = 1.532$ Å. The incident resolution was $\Delta\theta_{inc} \approx 0.2$ mradians, $\Delta\phi_{inc} \approx 0.4$ mradians with $\theta_{inc}$ and $\phi_{inc}$ defined as in Fig. 3. The vertical cross section of the beam at the sample was $w_{vert} = 0.5$ mm. A well-defined vertical beam is important because for saturated films the film thickness has a weak height dependence due to gravity. For example, at a height of 2.5 cm above a reservoir of liquid $^4$He, where the x-ray beam impinges on the sample, the thickness of the helium film should vary by $\sim 1.3$ Å over a change in height of 0.5 mm. The horizontal cross section $w_{hor}$ was confined so that the footprint of the beam would be smaller than the horizontal length $L_{sub}$ of the substrate, i.e., $w_{hor} < L_{sub}\sin(\theta_{inc})$. The maximum incident flux in a spot size of 0.25 mm$^2$ was $\approx 2.5 \times 10^8$ photons sec$^{-1}$ at NSLS. Details of the spectrometer used at the Harvard Materials Research Laboratory rotating anode are described elsewhere.[25]

The x rays enter the cryostat through three 0.001-in-thick Kapton windows and a 0.020-in.-thick beryllium window on the sample chamber [Fig. 2(a)]. In addition the x rays pass through several pieces of aluminized Mylar used as thermal radiation sheilding. After reflection from the substrate the beam exits through an identical set of windows. Altogether 30% of the beam intensity is lost upon passage through the cryostat.

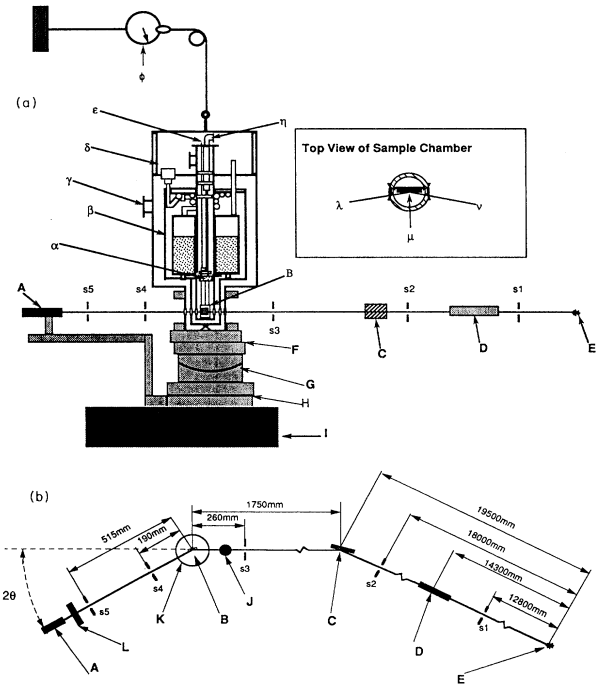


FIG. 2. (a) Schematic of experimental setup. $\alpha$: continuous fill pot; $\beta$: aluminum cold shield; $\gamma$: pumping port; $\delta$: helium exhaust; $\varepsilon$: helium dosing line; $\phi$: spring scale counterbalance; $\eta$: continuous fill pot pump port; $\lambda$: reflected x-ray beam; $\mu$: silicon substrate; $\nu$: incident x-ray beam. **A**: scintillation detector; **B**: sample chamber; **C**: germanium monochrometer; **D**: mirror; **E**: synchrotron electron ring; **F**: translation stages; **G**: tilt stage; **H**: rotation stages; **I**: optical table. (b) Scattering geometry at NSLS. **J**: beam mointor; **K**: cryostat; **L**: attenuator; other notations as in (a).

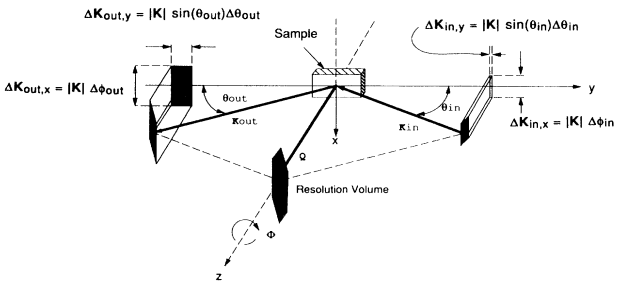


FIG. 3. Resolution geometry for specular reflectivity.

The outgoing arm of the spectrometer serves to define the outgoing resolution, and reduce the amount of stray scattering into the detector. To insure that the detector was operating in a linear range a series of calibrated copper foil attenuators ($L$) placed between $S5$ and the detector limited the maximum count rates to $\sim 4 \times 10^4$ photons sec$^{-1}$. Typical outgoing resolution was $\Delta\theta_{out} = 2$ mradians and $\Delta\phi_{out} = 6$ mradians.

The experimental cell within the cryostat consisted of a copper cylinder with a 0.275-in-thick wall connected to a room-temperature helium gas dosing system via a thin (0.016-in-i.d.) capillary dosing tube. The cell was equipped with two 0.020-in.-thick beryllium x-ray access windows. The substrates were $1.3 \times 0.7 \times 0.125$-in-thick Si wafers whose top surfaces were polished (001) or (111) planes. The (001) surfaces were coated with the native silicon oxide, typically $\sim 15$ Å thick, while the (111) surface was passivated with hydrogen.[31] The less complicated profile of the passivated (111) surface proved advantageous for these studies. The surface normal of the crystal, either (001) or (111), was oriented perpendicular to the $\Theta$-$2\Theta$ spectrometer axis.

Because of the finite angular resolution of the incident $(\Delta\theta_{inc}, \Delta\phi_{inc})$ and detected beams $(\Delta\theta_{out}, \Delta\phi_{out})$, the incident and outgoing wave vectors $\mathbf{K}_{inc}$ and $\mathbf{K}_{out}$ are distributed with some probability distribution $P_{1,2}(\mathbf{K})$ around the nominal spectrometer angles. Similarly, the wave-vector transfer $\mathbf{Q} \equiv \mathbf{K}_{out} - \mathbf{K}_{inc}$ is distributed about its nominal value with a probability distribution $\Xi(\mathbf{Q}) = \int P_1(\mathbf{K} - \mathbf{Q}) P_2(\mathbf{K}) d^3K$ where $\Xi(\mathbf{Q})$ defines the resolution of the spectrometer. For the present experiment it is sufficient to approximate the x rays as monochromatic, the beam profile as perfectly flat, and the slit edges as perfectly sharp. Thus the distributions of the incident and outgoing wave vectors $\mathbf{P}_1$ and $\mathbf{P}_2$ sketched in Fig. 3, define areas of equal probability from which the resolution function $\Xi(\mathbf{Q})$ is defined to be a volume of uniform probability density. Figure 3 depicts the relation between the size of the resolution volume, and the spectrometer angular divergences. Since $\Delta\theta_{out}$ and $\Delta\phi_{out}$

were significantly larger than $\Delta\theta_{\rm inc}$ and $\Delta\phi_{\rm inc}$ the uncertainty in $Q_x$ and $Q_y$ as determined by the projection of the resolution volume onto the $x,y$ plane is to good approximation determined solely by the projection of the outgoing resolution area fixed by the settings of $S5$. Typical values were

$$\Delta Q_x \approx |\mathbf{K}|\Delta\phi_{\rm out} \approx 2\times 10^{-2}\ \text{Å}^{-1}\ ,$$

$$\Delta Q_y \approx |\mathbf{K}|\sin(\theta)\Delta\theta_{\rm out}$$

ranging from $3\times 10^{-5}$ Å$^{-1}$ to $8\times 10^{-4}$ Å$^{-1}$. The x-ray coherence are used to define $\langle\rho(z)\rangle_{x,y}$, given by $\Delta x = 2\pi/\Delta Q_x \approx 300$ Å and $\Delta y = 2\pi/\Delta Q_y$, ranges from $2\times 10^5$ Å to $8\times 10^3$ Å. The effective specular resolution of the spectrometer $\Delta Q_z$, on the other hand, is much smaller than the vertical height of the resolution volume and is actually given by the length of the intersection of the resolution volume with the line $Q_x = Q_y = 0$ which is approximately given by

$$2|\mathbf{K}|\Delta\theta_{\rm inc} \approx 1.6\times 10^{-3}\ \text{Å}^{-1}\ .$$

Since the $z$-axis coherence length of approximately 8000 Å is much larger than the film thicknesses it is irrelevant. A more detailed discussion of correlation lengths and the effects of spectrometer resolution can be found in papers by Braslau *et al.*,[32] Schwartz *et al.*,[33] and Sanyal *et al.*[34]

### A. Helium films

Helium films were adsorbed onto the silicon substrate in two different ways. Saturated helium films were formed by admitting an amount of helium into the cell sufficient to form a 1–2-mm-high puddle of bulk helium liquid on the cell bottom. A helium film then formed on the substrate, either by adsorption from the vapor or by flow along the surface, such that the van der Waals attraction between the helium and the silicon just balanced the gravitational energy some distance above the puddle. This balance yields a film thickness $d(h)$ given by[35]

$$d(h) = (\gamma(d)/gh)^{\alpha}\ . \tag{3.1}$$

Here $\gamma(d)$ is the van der Waals force constant, $\alpha = \frac{1}{3}$ for nonretarded van der Waals forces, and $g$ is the gravitational acceleration. The weak thickness dependence of $\gamma$ results from retardation effects.[36]

The alternative method of adsorbing films was to condense the films from an unsaturated vapor of helium gas. The thickness of the film adsorbed on the substrate in this case is determined by the condition that the difference in chemical potentials between the unsaturated and saturated gases at the same temperature be equal to the shift arising from the van der Waals absorption potential at the surface of the adsorbed film. For low vapor pressures the chemical potential of the $^4$He vapor can be treated as though the gas was ideal, and the film thickness is determined by the condition

$$d_{\rm film} = \left[\frac{\gamma(d_{\rm film})}{k_B T \ln(P_{\rm sat}/P)}\right]^{\alpha}\ , \tag{3.2}$$

where $P_{\rm sat}$ is the saturation vapor pressure, and we have ignored the small contribution of gravity to $d_{\rm film}$. In practice, a fixed dose of gas is admitted into the sample cell, and then the cell is sealed off. As the temperature of the cell is reduced, the $^4$He vapor pressure drops and the film thickens.

### B. Saturated versus unsaturated films

In Fig. 4 we compare the results of a measurement on a typical saturated film (206 Å thick at 1.35 K) with those on a typical unsaturated film (193 Å at 1.13 K). Both were measured at NSLS at the same beam height position, and normalized to the Fresnel reflectivity for bulk silicon. Although the period of the oscillations (and hence the film thickness) is clearly defined in both cases, the amplitude of the oscillations at small $Q$ for the saturated film is only about 60% of that of the unsaturated film and decays more rapidly with increasing $Q$. In general, one can associate faster reflectivity decay with increasing $Q$ with larger roughness;[26] however, from Eq. (2.2) one can see that for either surface, in the limit that $Q \to 0$,

$$|\Phi(Q)| \to \left|(1/\rho_\infty)\int_{-\infty}^{\infty}(d\langle\rho(z)\rangle_{x,y}/dz)dz\right| = 1\ , \tag{3.3}$$

implying that unless the helium-vapor interface is exceptionally rough the amplitude of the oscillations is determined solely by the Fresnel reflectivities for the two layers. This is a known function of the helium and silicon bulk densities and should be the same for unsaturated and saturated films of comparable thickness. In order to explain the loss of amplitude for saturated films in terms of surface roughness, the roughness would have to have a component whose root-mean-square amplitude was of the order of $1/0.05 \approx 20$ Å, or larger. An alternative, although unphysical explanation would be if the density of the vapor at the liquid-vapor interface was as large as $\sim 30\%$ of the liquid density and decayed to the density of

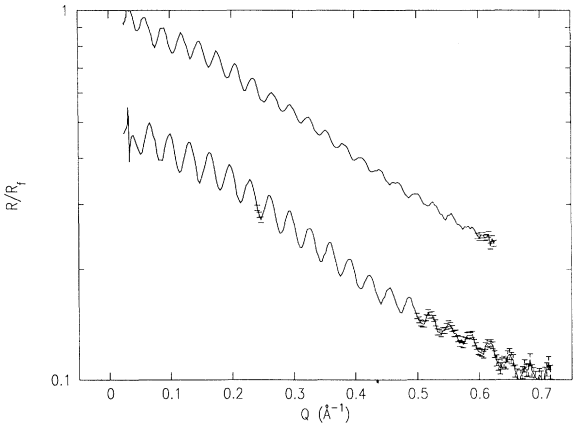


FIG. 4. Comparison of reflectivity from saturated and unsaturated films. (Top curve) $R/R_F$ for a 206-Å-thick saturated film measured at 1.35 K. (Bottom curve, multiplied by 0.5 for clarity) $R/R_F$ for a 193-Å-thick unsaturated film measured at 1.13 K.

the bulk vapor over a distance of the order of 20 Å or greater.

It is difficult to develop any plausible interpretation of this observation that would be consistent with the saturated film being in static equilibrium. We believe the most likely explanation is that the puddle gives rise to some macroscopic instability, possibly driven by external mechanical vibration resulting in macroscopic variations in the local film thickness ($\geq 10-20$ Å) that are fast on the time scale of an x-ray measurement (minimum time is of the order of seconds at small $Q$). Such temporal variations in the film thickness would "smear" the interference thus reducing the observable fringe amplitude.

In spite of this problem, as can be seen from Fig. 4, for thick films the period of the oscillations, which is a measure of the temporal and spatial average of the film thickness, is essentially identical to the period for films that are only slightly unsaturated. In our experience, covering many different experimental techniques, although it is often difficult to realize the theoretically expected amplitude for an interference signal, the period of the interference fringes are relatively insensitive to experimental errors. Consequently, we believe that the measured values of the period of the interference fringes from the saturated films yield reliable results for the average film thickness which, with Eq. (3.1), determine the van der Waals constant $\gamma(d)$ and exponent $\alpha$.

Measurements of film thickness at approximately constant height were made for saturated films at different temperatures using both the hydrogen passivated Si(111) surfaces as well as two separately prepared oxide coated Si(100) surfaces ($\sim 15$ Å $SiO_2$).[23] A summary of these results is presented in Table I. The value of the van der Waals exponent $\alpha$ was determined by measuring the variation in film thickness resulting from small changes in the height of the incident x-ray beam above the pool of liquid helium. Figure 5 shows a plot of $\ln(D)$ vs $\ln(h)$ where $d$ is the film thickness and $h$ is the height of the x-ray beam above the bulk puddle. The best fit to the data points (shown as the solid line) yields $\alpha=0.30\pm0.03$ for films approximately 200 Å thick. When $\gamma$ is regarded as a constant independent of $d$, $\alpha$ is expected to be somewhat smaller than $\frac{1}{3}$ due to retardation effects. Cheng and Cole,[36] however, define the van der Waals force constant by Eq. (3.1) with $\alpha\equiv\frac{1}{3}$. Using their definition we obtain

$$\gamma(d)|_{d\approx 200\ \text{Å}}=(1.2\pm0.1)\times10^3\ \text{K Å}^3$$

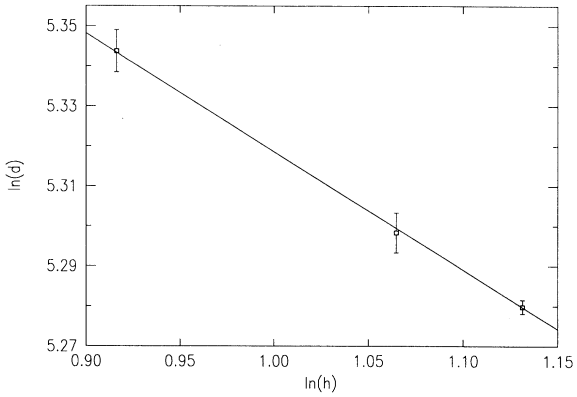


FIG. 5. Ln-ln plot of film thickness vs x-ray beam height. Best-fit line represents an exponent $\alpha=0.30\pm0.03$.

as compared with the theoretically predicted value of Cheng and Cole of $1.023\times10^3$ K Å$^3$. Our result is also in good agreement with the original calculation of Sabisky and Anderson of $1.00\times10^3$ K Å$^3$.[37] The discrepancy between the experimental and theoretical numbers is reduced when the phonon effects described by Cole, Swift, and Toigo are included.[38]

Although it is known for thin films that the effective van der Waals constant is sensitive to details of the surface termination,[39] it is not very surprising to observe that for $\sim$200-Å-thick films the oxidized (100) surfaces have approximately the same van der Waals constant as the hydrogen passivated (111) surface. In principal, the thickness dependence of $\gamma(d)$ could be measured over a much larger range of $d$ by studying unsaturated films as a function of the He vapor pressure; however, in the present measurement the vapor pressure in the cell was not known with sufficient accuracy.

## IV. METHOD OF FITTING THE DATA

Because of the stability problems with saturated films below the $\lambda$ point, mentioned above, and radiation induced changes in the thickness of films above the $\lambda$ point described further in Appendix A, the remainder of this paper focuses on unsaturated films on Si(111) at temperatures below the $\lambda$ point for which none of these problems were present. A summary of these results was presented

TABLE I. Film thickness as a function of height for saturated helium films adsorbed onto silicon substrates with differing surface preparation. Si(100)/$SiO_2$. Numbers 1 and 2 were two separate substrates prepared in an identical manner. For the entries with asterisks, the error refers to the height difference between this measurement and the measurement at 1.49 K.

| Substrate | $T(K)$ | $h$(mm) | $d$(Å) | $\gamma(d)(K-\text{Å}^3)$ |
|---|---|---|---|---|
| Passivated Si (111) | 1.13 | 25±2 | 215±1 | $1.2\pm1\times10^3$ |
| Si(100)/$SiO_2$ No. 1 | 1.25 | 25±2 | 213±1 | $1.2\pm1\times10^3$ |
| Si(100)/$SiO_2$ No. 2 | 1.35 | 31±0.5* | 196.0±0.3 | |
| | 1.35 | 29±0.5* | 200±1 | |
| | 1.49 | 25±2 | 209±1 | $1.1\pm1\times10^3$ |

by Lurio *et al.*[24] Figure 6(a) shows the measured reflectivity $R(Q)$ for helium films at four different temperatures, corresponding to four different film thicknesses. The bare silicon substrate reflectivity at 20 K is also shown for comparison. Figure 6(b) shows the same reflectivity curves, but normalized to the Fresnel reflectivity for bulk silicon, $R_F^{Si}(Q)$. The calculated reflectivities of model interfacial profiles which best represent the measured reflectivity data are depicted as solid lines in Fig. 6.

Theoretical treatments of correlations between substrate and free-surface structures of an absorbed film indicate that for sufficiently thick films the influence of short-wavelength substrate roughness of the free surface is negligible.[40] This prediction is supported by room-temperature studies of organic liquid films.[41] By similar reasoning, for films thicker than a few tens of angstroms, the local properties of the free surface should also be independent of the film thickness. As a result, models for the density profile at the solid-liquid and liquid-vapor interface can be constructed independently; this is the approach employed here. The model for the solid surface was constructed on the basis of x-ray reflectivity measurements performed on the dry substrate at 20 K, as well as independent x-ray photoelectron spectroscopy (XPS) and scanning tunneling microscopy (STM) measurements. This model was then modified slightly to describe the adsorption of helium onto the silicon surface by adding a solid helium layer at the interface[36,42] and allowing for interpenetration of the helium into the surface roughness of the substrate. In the next sections we describe the details of the construction of the model for the silicon surface and silicon-helium interface. Our presentation of the model for the helium liquid-vapor interface follows after this discussion.

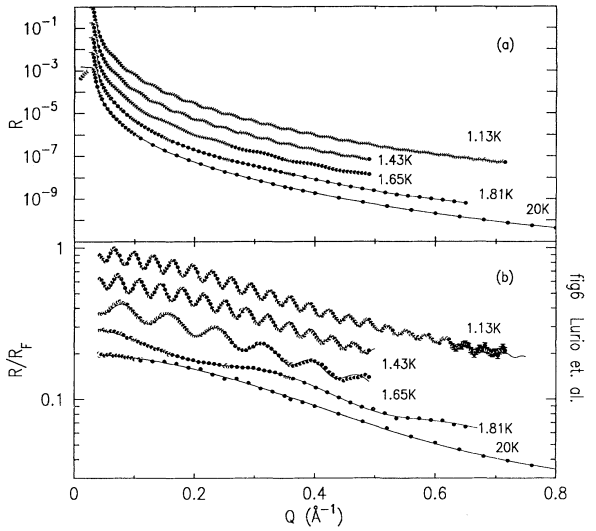


FIG. 6. (a) Measured reflectivity $R(Q)$ for a silicon substrate coated with several different unsaturated $^4$He films: Top to bottom: $T=1.13$ K, $d_{film}=192$ Å; $T=1.43$ K, $d_{film}=175$ Å; $T=1.65$ K, $d_{film}=80$ Å; $T=1.81$ K, $d_{film}=18$ Å; $T=20$ K without a film. Data are shown as circles; lines represent fits to data using the asech model convoluted with thermal capillary waves. Successive data sets are multiplied by 0.2 for clarity. (b) Same reflectivity data but normalized to the Fresnel reflectivity for bulk Si, $R_F^{Si}(Q)$.

### A. Substrate surface, and solid-liquid interface

Although the $Q$ dependence of the interference envelope of $R(Q)/R_F(Q)$ provides the absolute magnitude of the $^4$He-vapor scattering amplitude $|S_{He}(Q)|$ independent of any specific model for the Si-$^4$He interface, knowledge of the phase, $\phi_{He}(Q)$, is absolutely essential for a full determination of the $^4$He/vapor density profile. For this purpose it is necessary to obtain a model of the Si/$^4$He interface from which the phase $\phi_{Si}(Q)$ of $\Phi_{Si}(Q)$ can be predicted. The phase $\phi_{He}(Q)$ of $\Phi_{He}(Q)$ can then be extracted from the $Q$ dependence of the phase of the oscillations, i.e., from $\phi_{He}(Q)-\phi_{Si}(Q)$.

The substrate used for the measurement was the polished (111) face of a silicon single crystal that was prepared by a commercial silica gel polish[43] and an ammonium fluoride-hydrofluoric acid treatment which resulted in removal of the native $SiO_2$ layer and hydrogen passivation of the Si(111) dangling bonds.[31] The atomic scale structure of the bare Si surface was characterized through x-ray specular reflectivity measurements of $|\Phi(Q)_{bare}|$, STM images of the surface morphology in real space and XPS determinations of the surface chemistry and contamination.

#### *1.* STM

Figure 7 shows an STM image of the silicon substrate after removal from the experimental cell. Atomic resolu-

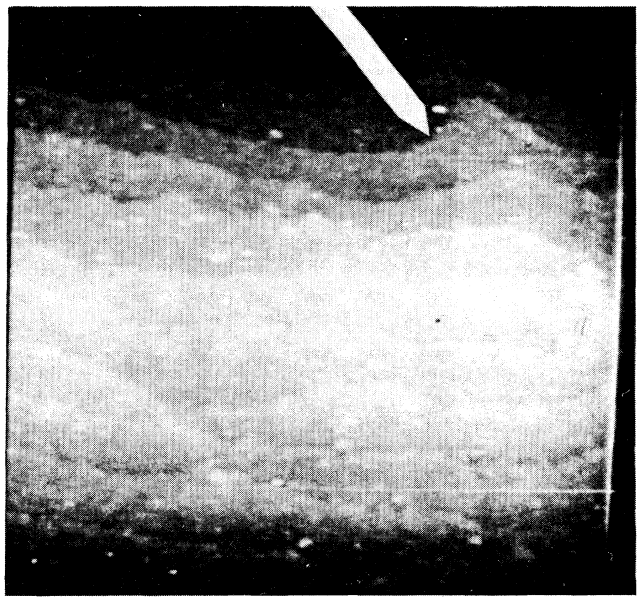

FIG. 7. STM image of hydrogen passivated Si(111) surface. This image was made after removing the substrate from the cryostat and a subsequent brief exposure to air. Although individual atoms are not visible terrace edges due to the crystal miscut can be clearly discerned (arrow).

tion was not obtained, possibly due to the difficulty of imaging the hydrogen passivation, the low contrast of the expected $1\times1$ reconstruction of the passivated surface, and the presence of surface contamination. Terrace step edges resulting from the crystal miscut ($\sim\frac{1}{4}°$) are clearly discernible. The image indicates that aside from contamination, the silicon surface consists of flat terraces ($\sim$300–400 Å wide) with somewhat wandering step edges.

### 2. XPS

XPS measurements were performed to probe both the quality of the hydrogen passivation and the nature of surface contamination. Comparison of the photoelectron spectra obtained from samples before and after the hydrogen passivation procedure indicates that the $Si^{+4}$ oxidation state peak is entirely removed to within the resolution of the measurement ($\sim$10% of the prepassivation integrated area) after surface passivation. To determine the amount of contamination present on the passivated sample surface a slightly more involved procedure was used. After the helium measurements were performed, the Si sample was transferred under dry nitrogen into an XPS spectrometer along with a thiol [$HS(CH_2)_2CH_3$] coated gold reference. A comparison of the integrated area of the XPS signals from the two substrates gave a measure of the areal density of carbon on the silicon surface (0.1 atom/Å$^2$). The amount of oxygen present on the surface could also be measured by reference to the carbon peak yielding 0.03 atoms/Å$^2$. The measured areal density of hydrocarbon and oxygen on the passivated Si surface is, however, only an upper bound since the contamination and oxidation will have increased in the interval between the x-ray measurement, and the XPS measurement (several months).

### 3. X-ray scattering

Using the STM and XPS results a trial model was constructed for the dry substrate surface density profile. The parameters representing the density profile were varied, within a small range about the initial estimate, to give the best fit of the calculated reflectivity of the model to the specular reflectivity data from the dry substrate. The results of this fit to the dry substrate density profile then served as the starting point for the model of the helium-wet substrate. The resulting density profiles for the silicon-helium interface, along with the initial guesses for the profile based on the STM and XPS measurements are shown in Fig. 8.

The model for the density profile due to the silicon termination (neglecting contamination) was constructed as follows. A three-dimensional surface map was generated from the STM image, with each terrace step edge corresponding to the 3.14 Å step height of silicon. A reference plane describing the mean surface height was fit to this map, and the variation of the local surface position about the reference plane was calculated. Because of the finite miscut between the Si surface and the Si(111) lattice, oscillations due to the lattice planes are washed out. The resultant distribution function for the density about the

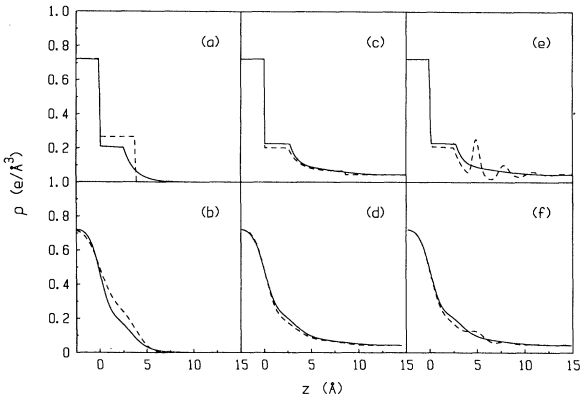


FIG. 8. (a) (— — —) Trial local density profile for the Si-C-vapor interface based on the XPS results (——) local-density profile obtained from the best fit to the dry silicon surface at 20 K. (b) The density profiles obtained by averaging the profiles in (a) over the height variations in the stepped (111) Si surfaces as obtained from the STM results. (c) (— — —) The trial local density profile for the Si-C-He interface obtained by adding two layers of solid helium and liquid helium to the best-fit profile in (a). (——) The local profile that provided the best fit to the 1.13 K data. (d) The profiles obtained by averaging the two profiles in (c) over the stepped Si surface. (e) Comparison between the best-fit local profile in (c) and the profile obtained by convolving the theoretical local-density profile proposed by Treiner[45] with the best-fit local-density profile for the Si-C-vapor interface in (a). (f) Profiles obtained by averaging the profiles in (e) over the Si height variations observed by STM.

average surface was well approximated by a Gaussian with $\sim$1 Å rms width. To account for the observation that the individual automatically flat terraces were coated with slightly less than one monolayer of carbon, we assumed that the *local* density profile consisted of an abrupt interface between a uniform material with the average electron density of crystalline silicon and a film of hydrocarbon that has a diffuse interface with the vacuum [Fig. 8(a), dashed line]. The local electron density of the substrate was given by

$$\rho_{\text{bare}}(z)=(\rho_{\text{Si}}-\rho_c)\Theta(z) +\rho_c\{\Theta(z-d_c)+\Theta(d_c-z) \times\exp[-(z-d_c)/\sigma_c]\} . \quad (4.1)$$

Here $z$ is the position along the local surface normal (i.e., not the miscut direction), $\Theta(z)$ is the theta function, $\rho_{\text{Si}}$ is the average electron density of bulk silicon, $\rho_c$ is the density of the hydrocarbon layer, $d_c$ is the thickness of the hydrocarbon layer, and $\sigma_c$ is the length scale of the hydrocarbon exponential decay. The *average* density profile relative to the reference plane [Fig. 8(b), dashed line] was then obtained by convoluting the local density profile of Eq. (4.1) with a Gaussian of width $\sigma_{\text{Si}}$:

$$\langle\rho_{\text{bare}}\rangle(z)\frac{1}{\sqrt{2\pi\sigma_{\text{Si}}^2}}\int_{-\infty}^{\infty}\rho_{\text{bare}}(t)\exp[-(z-t)^2/2\sigma_{\text{Si}}^2]dt . \quad (4.2a)$$

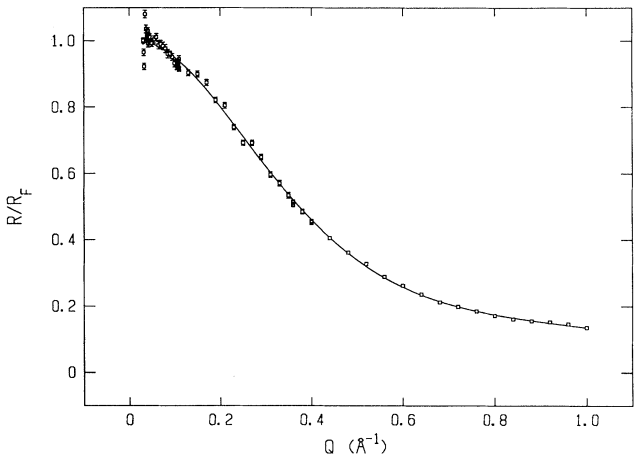


FIG. 9. $R(Q)/R_F^{\mathrm{Si}}(Q)$ for the bare silicon substrate at 20 K. Squares are data; line is best fit to bare substrate.

The reflectivity from this profile was then calculated using Eq. (2.1). The Fourier transform of this model [Eq. (2.2)] is then

$$\Phi_{\mathrm{bare}}(Q)=\exp(-Q^2\sigma_{\mathrm{Si}}^2/2) \times\left[\frac{(\rho_{\mathrm{Si}}-\rho_c)}{\rho_{\mathrm{Si}}}+\frac{\rho_c}{\rho_{\mathrm{Si}}}\exp(iQd_c)\frac{1}{1-iQ\sigma_c}\right]. \tag{4.2b}$$

Hence the predicted reflectivity is a function of the same parameters that describe the real space profile; i.e., $\rho_{\mathrm{Si}}$, $\sigma_{\mathrm{Si}}$, $\rho_c$, $d_c$, and $\sigma_c$. The solid line in Fig. 9 describes the best fit to the reflectivity from the bare substrate by allowing $\sigma_{\mathrm{Si}}$, $\rho_c$, $d_c$, and $\sigma_c$ to vary; $\rho_{\mathrm{Si}}$ was fixed to the bulk silicon electron density. The parameter values for the best fit are listed in Table II along with comparisons with the initial trial values, i.e., the silicon surface roughness $\sigma_{\mathrm{Si}}$ obtained from the STM picture, the hydrocarbon density $\rho_c$ of a bulk hydrocarbon (e.g., ethanol), and the upper bound on the total integrated contamination $\rho_c(d_c+\sigma_c)$ obtained from the XPS measurement. The local profile corresponding to this best fit to the specular reflectivity is shown in Fig. 8(a) (solid line) while the average of this "best-fit" local profile over the surface height variation of the silicon is depicted in Fig. 8(b), (solid line).

TABLE II. Results of fits to the dry and helium coated silicon substrate.

| Layer | Thickness (Å) | $\rho/\rho_{\mathrm{Si}}$ | $\sigma$(Å) |
|---|---|---|---|
| Trial parameters for dry substrate | | | |
| Hydrocarbon | 3.0 | 0.37 | 0.0 |
| Best-fit parameters for dry substrate | | | |
| Hydrocarbon | 2.3 | 0.28[a] | 1.03 |
| Trial parameters for helium-wet substrate | | | |
| Hydrocarbon | 2.3 | 0.28 | 1.03 |
| Solid $^4$He | 4.8 | 0.10 | 0.0 |
| Best-fit parameters for helium-wet substrate | | | |
| Hydrocarbon | 2.7 | 0.32[b] | 0.8 |
| Solid $^4$He | 4.9 | 0.12[c] | 2.5 |

[a]As compared with $\rho=0.37$ for bulk ethanol.
[b]This value may be larger than for the dry substrate due to interpenetration of the helium within the hydrocarbon.
[c]As compared with $\rho=0.061$ for bulk liquid helium.

As can be seen from the figures, the final best-fit values are reasonably close to the initial guess values.

#### 4. *Modifications for helium-wet surface*

When the substrate is wet with helium the density profile at the Si-$^4$He interface must be modified to include the liquid helium. In addition, there is expected to be some solidification of the first layers of the helium adjacent to the interface.[42,44] The model for the substrate with carbon contamination was modified by inclusion of a layer of solid helium such that, when the liquid $^4$He is included, the net result is a model with three layers: hydrocarbon contamination, solid $^4$He, and liquid $^4$He. The helium films measured in this experiment (excepting possibly the 18-Å-thick film) are all sufficiently thick that the local density profile at the $^4$He-vapor interface can be treated separately from density profile at the substrate-$^4$He interface. Hence the substrate-$^4$He interface can be represented by silicon coated with hydrocarbon and solid helium immersed in bulk liquid helium. The specific form of the model used is given by

$$\rho_{\mathrm{sub}}(z)=(\rho_{\mathrm{Si}}-\rho_c)\Theta(z)+(\rho_c-\rho_{s\mathrm{He}})\{\Theta(z-d_c)+\Theta(d_c-z)\exp[-(z-d_c)/\sigma_c]\} +(\rho_{s\mathrm{He}}-\rho_{l\mathrm{He}})\mathrm{erf}[(z-d_c-d_{s\mathrm{He}})/\sigma_{s\mathrm{He}}]+\rho_{l\mathrm{He}}\,. \tag{4.3}$$

Here $\rho_{s\mathrm{He}}$ and $d_{s\mathrm{He}}$ are the density and thickness of the solid helium layer and $\sigma_{s\mathrm{He}}$ is the solid-helium–liquid-helium interfacial width for this layer. The parameters $\rho_{l\mathrm{He}}$, $d_{l\mathrm{He}}$, and $\sigma_{l\mathrm{He}}$ are the analogous quantities for the liquid-helium layer and liquid-He vapor interface.

When fitting to the substrate-$^4$He interface, both the solid-liquid and liquid-vapor interface parameters were allowed to vary simultaneously. Although the dry silicon parameters were allowed to vary during the fit they all remained close to their initial values. The final values ob-

tained from the fit were quite close to the expected thickness and density of the solid helium layer. This is illustrated in Figs. 8(c) and 8(d) by the (dashed line) curves for the trial functions and (the solid line) for the final profiles. Table II also lists the initial trial values and final best-fit values for the parameters in this model. As before these parameters describe the local-density profile which was then convoluted with the average surface variation [e.g., Eq. (4.2)] using a value of $\sigma_{Si}=0.9$ Å.

Alternatively, we were able to obtain comparable results by using the theoretically predicted solid-helium profile of Treiner[45] in place of our three-parameter model for the solid-helium layer. Comparison between this model and the results of our model described above is illustrated in Figs. 8(e) and 8(f). Although the local-density profile is quite different for the two models, their surface averaged profiles are comparable.

As the preceding discussion has demonstrated, a complete description of the solid-liquid interface requires the use of multiple layers. Although the Fourier transform of this model is analytic, and hence the reflectivity at large $Q$ is easy to calculate, at small $Q$ multiple scattering and refraction must be taken into account. In this limit Eq. (2.3) was used recursively to successively replace the reflectivity from a given pair of interfaces, with a single "effective" interface. This is straightforward, and similar to the method originally used by Parrat for similar problems.[27]

### B. Model for helium liquid-vapor interface

In order to properly interpret these results it is important to realize that the measurements reported here were made above 1 K and the measured profiles are expected to be broader than the $T=0$ profile because of thermal excitation of the surface capillary waves (ripplons).[13] As a result the model that we use for the measured liquid-vapor density profile can be interpreted as the convolution of a $T=0$ "intrinsic" density profile $\rho_0(z)$, with a distribution function that represents "roughness" induced by thermally excited surface modes. At any finite temperature the local-density profile at the surface will be

$$\rho(x,y,z)=\rho_0[z-h(x,y),y,z] ,$$

where $h(x,y)$ represents the variation of the surface height due to thermal excitation. The thermally induced surface roughness can be calculated quite accurately below 2 K because only long-wavelength modes of the surface will be excited ( $>20$ Å), and at these wavelengths the liquid can be treated using bulk hydrodynamics of an incompressible fluid.[46] Similar calculations have successfully predicted the surface roughness of water at room temperature,[33] and recent neutron scattering measurements of helium films confirm the results of hydrodynamic treatment down to length scales as small as $\sim 3$ Å.[9] This method facilitates comparison between data taken at different temperatures and film thicknesses, since they should all yield consistent $T=0$ profiles. In addition, comparison with other experimental results obtained at different temperatures, and with theoretical work on the $T=0$ density profile can be made in a straightforward manner.

### C. Capillary-wave model

The thermal roughness of the surface was calculated using the classical dispersion relation for capillary-gravity waves (ripplons)[32] by replacing the gravitational field with the van der Waals surface field and the classical thermal occupation numbers by those given by Bose Einstein statistics. For a ripplon of frequency $\omega$ the dispersion relation is given by

$$\omega^2=(\nu/\rho)k(k^2+k_v^2)\tanh(kd) , \tag{4.4}$$

where $\nu$ is the surface tension, $\rho$ the mass density, $d$ the thickness of the liquid, $k$ is the mode wave vector ($k=2\pi/\lambda$), and

$$k_v^2\equiv[n\gamma/\alpha\nu d^{(1+1/\alpha)}] ,$$

where $n$ is the helium number density. The thermal capillary-wave amplitude for each quantized mode (excluding zero-point roughness) is given by

$$\frac{1}{2}\langle A_k^2\rangle=\frac{\langle n(E)\rangle\hbar\omega}{\nu(k^2+k_v^2)L^2} , \tag{4.5}$$

where $L$ is the size of the system and

$$\langle n(E)\rangle=[\exp(\hbar\omega/k_BT)-1]^{-1}$$

the Bose-Einstein occupation number. The mean-square deviation of the surface height is given by

$$\langle\sigma_{\rm cap}^2\rangle=\int_0^{k_{\max}}\tfrac{1}{2}\langle A_k^2\rangle N(k)d^2\mathbf{k} , \tag{4.6}$$

where $k_{\max}$ is crudely determined by the condition that the total number of surface modes is equal to the number of surface atoms (e.g., similar to the Debye theory of specific heat), and $N(k)=(2\pi/L)^2$ is the ripplon density of states. For films thicker than $\sim 15$ Å and temperatures around 1–2 K the integral is insensitive to the exact value for $k_{\max}$, and Eq. (4.6) can be approximately integrated yielding

$$\int_0^{k_{\max}}\langle A_k^2\rangle N(k)d^2k\approx\frac{k_BT}{2\pi\nu}\ln(k_Q/k_v) , \tag{4.7}$$

where $k_Q$ is defined as the wave vector for which $\hbar\omega(k_Q)=k_BT$, e.g., the quantum length scale cutoff. Table III gives the calculated values of the total capillary-wave roughness, as well as values for $k_v$, and $k_Q$ for the various films measured.

### D. Effects of resolution

As mentioned above, $\Phi(Q)$ is the Fourier transform of the $z$ derivative of the density $\rho(x,y,z)$, averaged over the projection of the x-ray coherence area on the plane of the surface. The finite x-ray coherence area results from the finite resolution of the spectrometer. Although any surface roughness will cause x rays to be scattered away from the specular beam, if the length scale of the surface roughness is sufficiently large the scattered radiation can

TABLE III. Predicted value of rms capillary wave roughness ($\sigma_{cap}$) as a function of film thickness and temperature. Also shown are the values for $k_v$ and $k_Q$ the van der Waals and quantum wave-vector cutoffs. The asterisk is the value of $\sigma_{cap}$ for this film had to be integrated numerically.

| $d_{film}$ (Å) | $k_v$ (Å$^{-1}$) | $k_Q$ (Å$^{-1}$) | $\sigma_{cap}$ (Å) |
|---|---|---|---|
| 192±1 | $7.7\times10^{-5}$ | 0.21 | 2.03 |
| 175±2 | $1.1\times10^{-4}$ | 0.24 | 2.30 |
| 80±2 | $3.3\times10^{-2}$ | 0.28 | 2.16 |
| 18±3 | 4.4 | $1.3\times10^{-3}$ | 1.4* |

still fall within the angular resolution of the spectrometer. Consequently the measured x-ray reflectivity is not decreased by long-wavelength fluctuations in the height of the surface. The situation is slightly more complicated for layered surfaces, like the one considered here, in which two interfaces are separated by a thickness $D(x,y)$. In this case the amplitude of the oscillations in the interference term can be sensitive to long-wavelength fluctuations in $D(x,y)$. For example, the measured intensity at some wave vector $Q$ is equal to the sum of the signals separately reflected form the two interfaces, which are not sensitive to long-wavelength fluctuations, plus an interference term that has the form $\sim\cos[QD(x,y)+\varphi]$. Even if the variations in $D(x,y)$ occur over distances that are large compared to the x-ray correlation length, variation in the phase of the cosine term for reflection from distant parts of the sample, $Q\delta D(x,y)$, will reduce the observed interference amplitude. On the other hand, if the fluctuations in the heights of the two surfaces are correlated, $D(x,y)$ will be constant over the length of the surface and there will be no reduction of the amplitude. Robbins, Andelman, and Joanny have provided a detailed theoretical discussion demonstrating that although the free surface of the adsorbed film will follow very long-wavelength fluctuations in the height of the substrate surface, the height of the free surface cannot follow fluctuations with wavelengths smaller than some critical length that depends on the film.[40] In the case of helium films this length scale is given by $\sim 2\pi/k_v$. Not surprisingly, this is the same length scale at which the helium surface waves on finite thickness films go from being primarily van der Waals in nature to primarily capillary in nature. For $^4$He films $\sim$175 Å thick, $2\pi/k_v \sim 60\,000$ Å, which is longer than the x-ray coherence length for $Q > \sim 0.01$ Å$^{-1}$. In principal, the amplitude of the interference term can be calculated correctly if the average over the coherence length $\langle\rho(z)\rangle_{x,y}$ used in calculating $\Phi(Q)_{Si}$ and $\Phi(Q)_{He}$ is replaced by an average over the critical length $2\pi/k_v$. However, x-ray reflectivity only gives an independent measure of $\Phi(Q)_{Si}$, which is determined from an average over the x-ray coherence length.

Direct interpretation of the present measurements would be seriously compromised if a significant fraction of the roughness of the silicon surface arose from harmonic components with wavelengths in the range between $2\pi/k_v \sim 60\,000$ Å and the x-ray coherence length $\sim$8000 Å. It seems unlikely, however, that a surface that has been macroscopically polished, and which is nearly atomically flat over length scales from 1 to 8000 Å, should be very rough over length scales from 8000 to 60 000 Å.

### E. Zero-kelvin density profile

The form found convenient for representing the $T=0$ profile of the $^4$He-vapor profile is a two-parameter function whose derivative is given by an asymmetric hyperbolic secan (asech):

$$\frac{d\langle\rho\rangle_0}{dz} = C/[\exp(az)+\exp(-bz)]\ ,$$
$$a=[1+\exp(-\eta)]/(2\sigma_0),\quad b=[1+\exp(\eta)]/(2\sigma_0)\ . \tag{4.8}$$

Here $\sigma_0$ is a measure of the interfacial width, $\eta$ is a parameter that reflects the asymmetry of the interface, and $C$ is fixed such that

$$\int (d\langle\rho\rangle/dz)dz = \rho_{l\mathrm{He}}\ .$$

Since the capillary waves are an incoherent superposition of many modes the average profile at finite temperature is obtained by convoluting this $T=0$ profile with a Gaussian whose second moment is just the mean-square deviation of the surface height due to thermal capillary waves. Hence,

$$\frac{d\langle\rho\rangle_{He}}{dz}(z,d_{film},T) = \frac{1}{(2\pi\sigma^2_{cap^{-\infty}})^{1/2}}\int_{exp}^{\infty}(-z'^2/2\sigma^2_{cap})\frac{d\langle\rho(z'-z)\rangle_0}{dz}dz'\ . \tag{4.9a}$$

The Fourier transform of this, used to generate the predicted reflectivity from the liquid vapor interface is then

$$\Phi_{He}(Q) = \frac{\{1-\exp[-2\pi ia/(a+b)]\}\exp(-Q^2\sigma^2_{cap}/2)}{\exp([\pi q/a+b)]-\exp[-\pi(2ia+q)/(a+b)])}\ . \tag{4.9b}$$

The choice of the asech form for $d\langle\rho\rangle_0/dz$ stems from the result of density functional theory which predicts that the $T=0$ density profile has an exponential decay into the bulk liquid and vapor, but not necessarily with equal length scales.[14] The asech form shares the same general features of the Fermi function that is typically used to parametrize $\rho_0(z)$. In particular, with suitable choice of $\eta$ and $\sigma$ this form can be made to produce the theoretical

profiles of Nayak, Edwards, and Masuhara,[5] Stringari and Treiner,[14] and Osborne.[22] For the present analysis the analytic Fourier transform of the asech form greatly simplifies the process of relating the predicted reflectivity to the model for the density profile [e.g., Eq. (2.2)].

Using the form of Eq. (4.9) to represent the finite-temperature density profile makes extracting the $T=0$ component of the density profile trivial. When fitting the theoretical form to the experimental data only the parameters $\eta$ and $\sigma_0$ of Eq. (4.8) are varied while $\sigma^2_{\rm cap}$ is fixed from the capillary-wave calculation. When values are obtained for the best fit, these are substituted directly into Eq. (4.8) to yield the zero-kelvin profile.

## V. RESULTS

The values of the parameters $\sigma_0$ and $\eta$ describing the liquid-vapor interface that gave the best fit to the reflectivity as determined by the minimum $\chi^2$ (typical $\chi^2 \sim 0.9$) are given in Table IV. These values were used to generate the fits in Fig. 6. As mentioned above, the values for the parameters describing the solid-liquid interface were also allowed to vary during the fit, but did not change significantly as shown in Fig. 8. The method used to determine the confidence limits given in this table are detailed in Appendix B.

Figure 10(a) illustrates $d\langle\rho\rangle/dz$ obtained from the best fit to the measured reflectivity data at 1.13 K. Figure 10(b) illustrates the extrapolated $T=0$ value of $d\rho/dz$ obtained by excluding the thermal capillary-wave roughness. Finally, Fig. 10(c) illustrates the $T=0$ density profile obtained by integrating the profile in Fig. 10(b). The confidence limits on these profile shapes obtained for the finite-temperature measurements and the $T=0$ extrapolation are indicated in Fig. 11. Of course, true confidence limits comprise a family of curves while Fig. 11 only depicts two representative members of this family. The details of how confidence limits were obtained for the values of $\sigma_0$ and $\eta$ is described below.

## VI. REAL SPACE PROFILES AND DISCUSSION

Figure 12 shows a comparison of our predicted $T=0$ density profile with several previously published theoretical models. Our predicted zero-K profile gives good agreement with the interfacial profile predicted by Stringari and Treiner.[14] The overall interfacial widths are comparable and, in addition, their profile predicts similar asymmetries. Note, however, that the uncertainty in our determination of the interface asymmetry is quite large due to uncertainties in the phase of the complex scattering amplitude for the silicon-helium interfacial profile. In particular, although the best fit is obtained for an asymmetric profile the data do not absolutely exclude

TABLE IV. Results of fits to data at several different temperatures and film thicknesses. Shown are the values of the parameters for the asymmetric hyperbolic secant fit convoluted with the capillary-wave roughness in Table III. Only the data at 1.13 K had sufficient range to determine $\eta$ hence the value of $\eta$ was fixed at the value obtained from this data set for all other temperatures.

| $T$ (K) | $\sigma_0$ (Å) | $\eta$ | $d_{\rm film}$ (Å) |
|---|---|---|---|
| 1.13 | 1.97±0.22 | $-1.1(+1.1,-\infty)$ | 192±1 |
| 1.43 | 1.84±0.17 | −1.1 fixed | 175±2 |
| 1.65 | 1.63±0.23 | −1.1 fixed | 80±2 |
| 1.81 | 2.01±0.22 | −1.1 fixed | 18±3 |

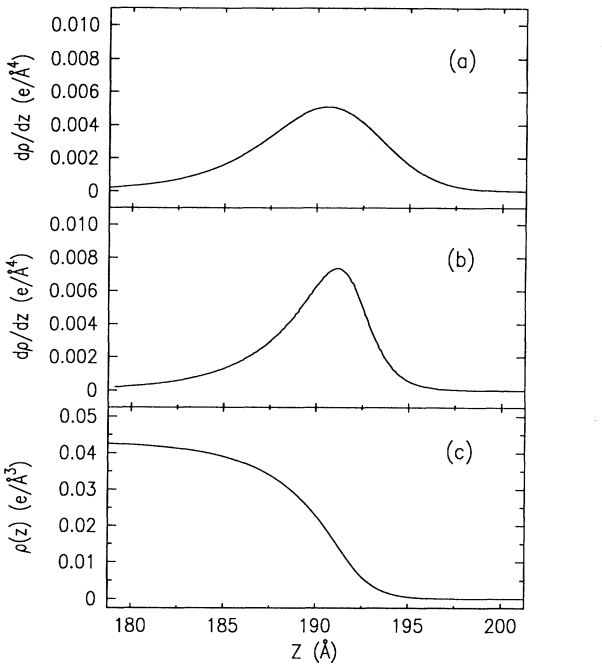


FIG. 10. (a) $d\langle\rho\rangle/dz$ obtained from best fit to specular reflectivity at 1.13 K. (b) $T=0$ value of $d\rho/dz$ obtained by excluding the capillary-wave roughness in (a). (c) Extrapolated $T=0$ density profile obtained from the integral of the profile in (b).

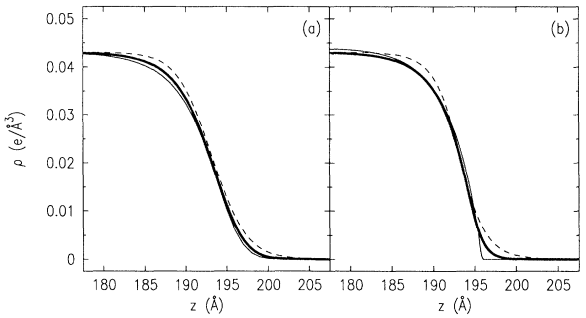


FIG. 11. (a) Illustration of the confidence limits on density profile from best fit to the specular reflectivity at 1.13 K. Light solid and dashed lines represent 95% confidence limits on the asymmetry of the profile, and give an indication of the range of allowable profiles that could fit the data. (b) Extrapolation to zero K of the profiles in (a) made by excluding the thermal capillary-wave roughness term in Eq. (4.9).

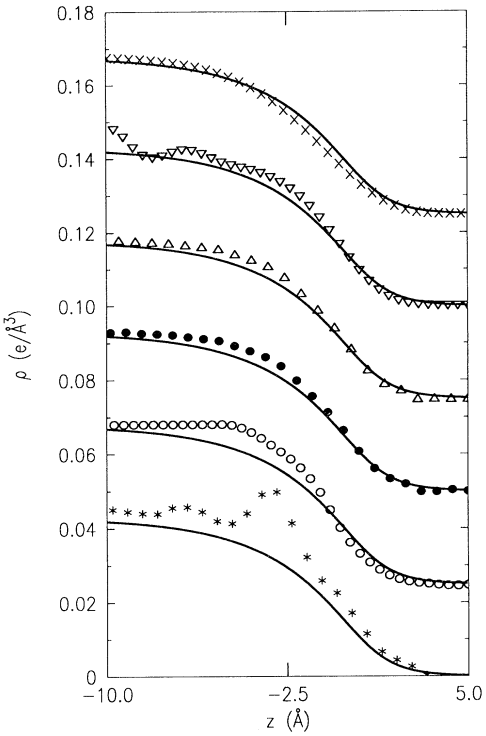


FIG. 12. Comparison of various theoretical profiles with our best-fit model. (——) and (*) F. D. Mackie and Chia-Wei Woo (Ref. 20); (○) Valles and Schmidt (Ref. 18); (●) Pieper and Wiringa (Ref. 17); (△) Krishna and Whaley (Ref. 19); (▽) Epstein and Krotscheck (Ref. 15); (×) Stringari and Treiner (Ref. 14). Successive models have been offset by 0.025 for clarity.

the possibility of a symmetric profile (see Table I). Although the qualitative agreement, evident in Fig. 12, between our results and some of the other theories are also not bad, they all tend to have narrower (90–10%) widths. Some part of this discrepancy may result from different treatment of the zero-point motion of capillary-wave modes.[13] Stringari and Treiner have included an additional term to account for the zero-point contribution to the surface tension which significantly broadens the profile.[14] Their *ad hoc* addition of a zero-point motion term leads to some confusion over what length scale in the plane of the surface the density profile is averaged over. Our measured profiles include all capillary-wave induced surface roughness with wave vectors larger than the van der Waals cutoff induced by the substrate. Although our $T=0$ extrapolation removes the thermal capillary-wave roughness it still includes the zero-point contribution.

A possible objection to the $T=0$ density profile extracted from our finite-temperature measurements is that other temperature-dependent effects on the surface width in addition to thermally excited capillary waves may be important. While the measurements at elevated temperatures (e.g., 1.65 K) may include such effects, we do not see any basis for suspecting the extrapolation from the 1.13 K data since this temperature is too low to significantly excite any modes other than capillary waves. This assertion is supported by the observation that the $^4$He bulk density and bulk isothermal compressibility both change by less than 0.5% between $T=0$ and 1 K. In addition, there is almost no change in the surface tension of the liquid between $T=0$ and 1 K other than that expected from thermal capillary waves.[47] Recently the density functional theory of Stringari has been extended to finite temperature by Guirao *et al.*[48] who find almost no change in the surface width up to 1 K. Their treatment, however, does not include the roughness effects of thermal capillary waves which broadens our profile from 7.6 Å at $T=0$ to 9.2 Å at 1.13 K. Indeed for a bulk liquid this thermal capillary wave roughness diverges in the absence of van der Waals or gravitational cutoff. In any case our finite-temperature measurements should certainly be an upper bound on the $T=0$ interfacial width.

With regards to previous experimental measurements we compare our results with the ellipsometry measurement of Osborne[22] and the atomic scattering measurements of Nayak, Edwards, and Masuhara.[5] For the case of ellipsometry a parameter $\eta_e$ is measured which is related to the density profile by[22]

$$\eta_e = \int_{-\infty}^{\infty} [(\varepsilon-\varepsilon_1)(\varepsilon-\varepsilon_2)/\varepsilon] dz \ , \tag{6.1}$$

where $\varepsilon$ is the dielectric constant of the helium as a function of $z$, while $\varepsilon_1$ is the bulk liquid dielectric constant and $\varepsilon_2$ that of the bulk vapor. If our measured density profile is used in Eq. (6.1) we obtain $\eta_e = 0.69\times10^{-12}$ m, as compared with Osborne's measured value of $0.67\pm0.1\times10^{-12}$ m. The agreement between the two measurements is excellent. A slight difficulty in making this comparison is that the surface area over which the density profile is averaged is not obvious from the ellipsometry measurements. For the free surface the total width has a logarithmic dependence on surface area and therefore this is not a significant correction.[32]

Atomic scattering measurements by Nayak, Edwards, and Masuhara, however, indicate a density profile with a 90–10% width of 4 Å at $T=0.02$ K.[5] This is significantly smaller than our $T=0$ extrapolation. The discrepancy may result from a temperature dependence of the interfacial width other than the subtracted thermal capillary waves contribution; however, as argued above we think this improbable. Another possible source for the discrepancy is that the atomic scattering measurements are most sensitive to the vapor side tail of the density profile. If we compare just the vapor side of the interface our best-fit profile gives a 50–10% width of 2.6 Å, due to the asymmetry of the interface. This is in reasonable agreement with the width measured by Nayak, Edwards, and Masuhara.[5]

## VII. CONCLUSIONS

We have measured the liquid-vapor interfacial density profile for helium films adsorbed onto an atomically flat silicon substrate over a range of temperatures and film thicknesses. Although there were difficulties with the measurements on normal fluid and saturated superfluid

films, unsaturated superfluid films were reliably used to characterize the superfluid $^4$He-vapor interfacial profile. The lowest-temperature measurement at 1.13 K yielded an asymmetric profile with a 90–10 % interfacial width of 9.2±1 Å. The $T=0$ interfacial profile extrapolated from this measurement using the theory of thermally excited ripplons has an interfacial width of $7.6^{+1}_{-2}$ Å and shows an asymmetry with the vapor side tail of the interface sharper than the liquid side tail.

## ACKNOWLEDGMENTS

We wish to thank Hans Biebuyck for assisting with the x-ray photoelectron spectroscopy and Ing-Shouh Hwang for assisting with the scanning tunneling microscopy measurement. This research was supported by Grant Nos. NSF-DMR-89-20490 and NSF-DMR-91-13782. NSLS, Brookhaven National Laboratory is supported by DOE Contract No. DE-AC02-76CH00016.

## APPENDIX A: FILMS ABOVE THE LAMBDA POINT

In addition to measurements performed on films of superfluid He II, measurements were also performed on normal fluid helium films. Above $T_\lambda$ the film thickness was sensitive to incident x-ray flux densities in excess of $10^8$ photons $cm^{-2}$ $sec^{-1}$ ($\sim 0.1$ $\mu W$ $cm^{-2}$). For the maximum incident flux density of $10^{10}$ photons $cm^{-2}$ $sec^{-1}$ the film thickness decreased from 215 to 63 Å. This thinning is comparable to the calculated effect on an unsaturated film if the substrate temperature is $\Delta T \sim 0.01$ K greater than the vapor. Thinning occurred approximately exponentially with time after turning on the x-ray beam, having a time constant $\sim 0.5$ sec. By contrast, the superfluid film thickness was independent of incident flux.

Considering that the principal difference between superfluid and normal films is that excess heat is rapidly carried away by superfluid flow, the differing behavior across the lambda point suggests that the film thinning is a thermal effect. Nevertheless, in view of the extremely small x-ray heat load it is difficult to rationalize the $\Delta T \sim 0.01$ K required for the film thinning observed above the lambda point. Almost none of the energy of the incident x rays is absorbed in the 200-Å-thick helium films itself since the absorption length of liquid helium is $\sim 18$ cm for 8.0 keV x rays, and the film is only 200 Å thick. Rather the x rays penetrate into the silicon substrate and are absorbed over a depth of $\mu \sin(\theta)$ where $\theta$ is the angle of incidence and $\mu$ the absorption length of the silicon. For the largest angle at which the thinning of the normal fluid film was observed ($\theta = 1.4°$) this corresponds to a depth of $1.5 \times 10^4$ Å. Direct heating of the substrate cannot be the thinning mechanism since if all the heat is absorbed in this layer in the silicon the calculated local temperature gradient based on the known thermal conductivity of silicon[49] is three orders of magnitude too small. Furthermore, if it is some sort of thermal mechanism it must be fairly efficient in transferring energy to the $^4$He film since thinning the film from 200 to 63 Å with the incident x-ray flux of $1 \times 10^{-5}$ W $cm^{-2}$ in 0.5 sec requires that approximately 50% of the x-ray energy goes into heating the helium.

With just the information available from the x-ray measurements it is difficult to determine the exact mechanism by which the normal fluid films thin. We will briefly sketch one hypothesis for a mechanism. Since the absorption length of the photoelectrons produced by the x rays is comparable to the x-ray penetration depth a sizable fraction of the photoelectrons escape the silicon substrate surface. These electrons deposit their energy in the helium film and in the helium vapor within the first millimeter or so above the film. In view of the relatively low thermal conductivity of $^4$He vapor, we calculate that this energy should lead to a thermal gradient in the vapor of a few millikelvin. By this mechanism the warmer vapor then heats the helium film and consequently thins it. As mentioned above, we calculate that the temperature difference between the substrate and the vapor required for the observed film thinning is $\sim 0.01$ K. This temperature difference is crudely consistent with the steady difference (0.08 K) predicted from the thermal conductivity of helium gas at the temperature measured (2.35 K) and the incident x-ray heat load. It is not clear, however, why this thermal gradient is not shorted to the substrate. Although large Kapitza resistances of order 20 $cm^{-2}$ K $W^{-1}$ have previously been reported between a helium film coated copper substrate and helium vapor,[50] to explain our results a Kapitza resistance of order 800 $cm^2$ K $W^{-1}$ is required. This is more than an order of magnitude larger than most measured values for the Kapitza resistance;[51] however, it is roughly consistent with the Kapitza resistance expected on the basis of the theory of Khalatnikov.[52] Perhaps the agreement of the present results with the theoretical predictions is due to the exceptionally clean and flat surfaces used. Below the lambda point of course any heating effect is shorted out by the film flow.

## APPENDIX B: ERROR ANALYSIS

In principal, the confidence limits $(\Delta\sigma_0, \Delta\eta)$ on the parameters $\sigma_0$ and $\eta$ could be determined from the contours that cause the reduced $\chi^2$ to increase above the minimum value by a specified amount. In the present experiment, however, this criteria could not be applied because systematic errors in the measured reflectivity were comparable to the uncertainty due to photon statistics (typically $<0.5\%$). This systematic uncertainty results from a combination of factors associated with the large dynamic range ($\sim 10^9$) of the measurement. For example, systematic errors are introduced via the scale factors used to normalize data subsets collected with the different incident slit and attenuator configurations required for the extended dynamic range. Similarly, direct beam normalization and sample alignment uncertainties contribute to the systematic error. Fortunately, the interference scattering geometry facilitates the estimation of model confidence levels despite the systematic errors since the

$^4$He surface structural information is encoded in the oscillations of period $2\pi/d_{\text{film}}$.

The procedure employed is illustrated pictorially in Fig. 13. The value of $\chi^2$ is minimized for a series of fixed values of the parameter of interest through variation of the remaining parameters of the model. The confidence limits for this parameter are determined through examination of the Fourier transform of the fit residuals for each value of the fixed parameter. For the example in Fig. 13 we display the confidence limits of the parameter $\sigma_0$ using the data set measured at 1.13 K. The residuals defined by

$$E(Q)=[R(Q)-R_{\text{Fit}}(Q)]/R_{\text{Fit}}(Q) \tag{B1}$$

of two such fits are plotted in Figs. 13(a) and 13(b). The absolute squares of the Fourier transform of these residuals

$$|\tilde{E}(Z)|^2=\left|\frac{1}{2\pi}\int_{-\infty}^{\infty}E(Q)e^{-iQZ}dQ\right|^2 \tag{B2}$$

are depicted in Figs. 13(c) and 13(d).

For an imperfect fit [Figs. 13(b) and 13(d)] there is a peak in $|\tilde{E}(Z)|^2$ at $Z=d_{\text{film}}$ which stems from the poor fit of the interference oscillations. To judge the quality of a fit, we evaluate the probability that the square of the absolute value, $|\tilde{E}(Z)|^2$ in the vicinity of $d_{\text{film}}$ is consistent with the (presumed) random fluctuations in $|\tilde{E}(Z)|^2$ over the rest of the interval. Explicitly, we take

$$U^2_{\text{film}}\equiv\langle|\tilde{E}(Z)|^2\rangle,\quad |Z-d_{\text{film}}|\le\Delta\ , \tag{B3a}$$

$$U^2_{\text{rnd}}\equiv\langle|\tilde{E}(Z)|^2\rangle,\quad |Z-d_{\text{film}}|>\Delta\ , \tag{B3b}$$

where $\Delta$ is chosen (somewhat arbitrarily) to be 30 Å. We define the confidence limit for the parameter $p_i$ as the value of $p_i$ such that $U^2_{\text{film}}=2U^2_{\text{rnd}}$. If the random errors followed Gaussian statistics this condition would imply that the probability of $U^2_{\text{film}}$ resulting from random errors was $\sim 5\%$. This criterion can only be applied if $U^2_{\text{film}}\approx U^2_{\text{rnd}}$ for the best-fit value of $p_i$. This was indeed the case for most of the data sets. For the data set at 1.65 K, however, the fit was somewhat poorer. In this case we chose for the confidence limit the condition $U^2_{\text{film}}=2U^2_{\text{film-min}}$ where $U^2_{\text{film-min}}$ was the smallest value obtained for $U^2_{\text{film}}$.

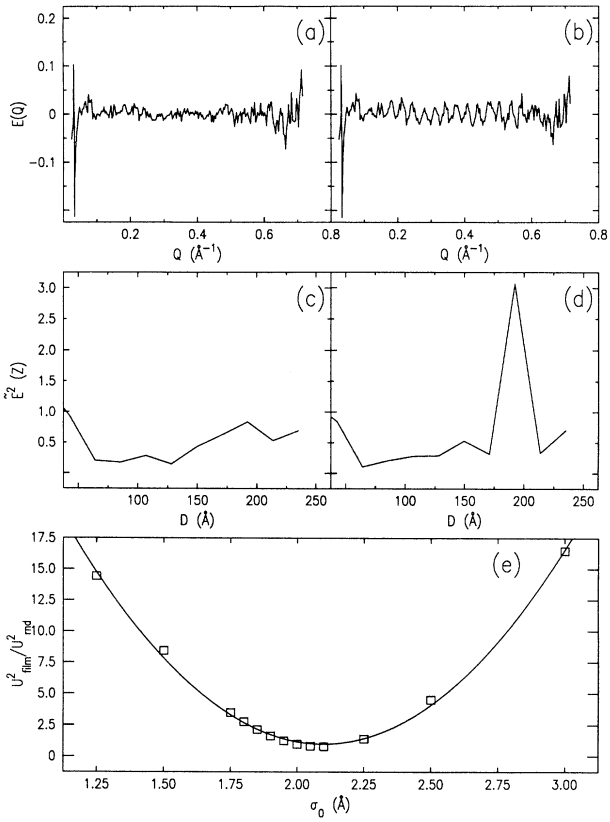


FIG. 13. Schematic illustration of error analysis procedure. (a) Residuals $E(Q)$ for fit to 1.13 K data set with $\sigma_0=2.0$ and the remaining variables in the model floated. (b) $E(Q)$ with $\sigma_0=1.5$. (c) Absolute square of Fourier transform of residuals $|\tilde{E}(Z)|^2$ for $\sigma_0=2.0$. (d) Absolute square of Fourier transform of residuals $|\tilde{E}(Z)|^2$ for $\sigma_0=1.5$. (e) $U^2_{\text{film}}$ as a function of $\sigma_0$, with parabola fit ( —— ).

*Present address: Rensselaer Polytechnic Institute, Dept. of Physics, Troy, New York, 12180-3590.

†Present address: IBM Research Division, Almaden Research Center, K33-801, 650 Harry Road, San Jose, CA 95120-6099.

[1]V. L. Ginzburg and L. P. Pitaevski, Zh. Eksp. Teor. Fiz. **34**, 1240 (1958) [Sov. Phys. JETP **7**, 858 (1958)].

[2]W. Brouwer and R. Pathria, Phys. Rev. **163**, 200 (1967).

[3]C. A. Croxton, *Statistical Mechanics of the Liquid Surface* (Wiley, New York, 1980).

[4]J. J. Berkhout, O. J. Luiten, I. D. Setija, T. W. Hijmans, T. Mizusaki, and J. T. M. Walraven, Phys. Rev. Lett. **63**, 1689 (1989).

[5]V. U. Nayak, D. O. Edwards, and N. Masuhara, Phys. Rev. Lett. **50**, 990 (1983).

[6]M. Cole, Rev. Mod. Phys. **46**, 451 (1974).

[7]I. F. Silvera and J. T. M. Walraven, *Spin Polarized Atmoic Hydrogen*, edited by D. F. Brewer (North Holland, Amsterdam, 1986), Vol. X, p. 139.

[8]M. Himbert and J. Dupont-Roc, J. Low Temp. Phys. **76**, 435 (1989).

[9]H. J. Lauter, H. Gofrin, V. L. P. Frank, and P. Leiderer, Phys. Rev. Lett. **68**, 2484 (1992).

[10]A. C. Forbes and A. F. G. Wyatt, Phys. Rev. Lett. **64**, 1393 (1990).

[11]S. R. Bandler, R. E. Lanou, H. J. Maris, T. More, F. S. Porter, G. M. Seidel, and R. H. Torii, Phys. Rev. Lett. **68**, 2429 (1992).

[12]K. R. Atkins, Can. J. Phys. **31**, 1165 (1953).

[13]M. W. Cole, Phys. Rev. A **1**, 1838 (1970).

[14]S. Stringari and J. Treiner, Phys. Rev. B **36**, 8369 (1987).

[15]J. L. Epstein and E. Krotscheck, Phys. Rev. B **37**, 1666 (1988).

[16]E. Krotscheck, S. Stringari, and J. Treiner, Phys. Rev. B **35**,

4754 (1987).
[17]S. Pieper, R. Wiringa, and V. R. Pandhari, Phys. Rev. B **32**, 3341 (1985).
[18]J. Valles and K. Schmidt, Phys. Rev. B **38**, 2879 (1988).
[19]M. V. R. Krishna and K. B. Whaley, J. Chem. Phys. **93**, 6738 (1990).
[20]F. D. Mackie and C.W. Woo, Phys. Rev. B **18**, 529 (1978).
[21]D. O. Edwards, Physica **109&110B**, 1531 (1982).
[22]D. V. Osborne, J. Phys. Condens. Matter **1**, 289 (1989).
[23]I. M. Tidswell, B. M.Ocko, P. S. Pershan, S. R. Wasserman, G. M. Whitesides, and J. D. Axe, Phys. Rev. B **41**, 1111 (1990).
[24]L. B. Lurio, T. A. Rabedeau, P. S. Pershan, I. F. Silvera, M. Deutsch, S. D. Kosowsky, and B. M. Ocko, Phys. Rev. Lett. **68**, 2628 (1992).
[25]L. Lurio, Ph.D. thesis, Harvard, 1992 (unpublished).
[26]P. S. Pershan, Faraday Discuss. Chem. Soc. **89**, 231 (1990).
[27]L. G. Parrat, Phys. Rev. **95**, 359 (1954).
[28]The precise range in $Q$ needed to resolve structural details of a given size depends on the kind of structure that is of interest. To resolve the overall length scale "$d$" of the interfacial profile requires measurements of $R(Q)$ out to approximately $Q=1/d$. On the other hand, to resolve oscillatory structure of wavelength $\lambda$, requires measurements of $R(Q)$ out to approximately $2\pi/\lambda$.
[29]J. D. Jackson, *Classical Electrodynamics* (Wiley, New York, 1975).
[30]Bulk diffuse scattering from helium is a more severe problem than for many other liquids for two principle reasons. Liquid helium has more long-wavelength density fluctuations than most other liquids which leads to a larger than normal structure factor at small $Q$, and the extinction length in helium is $\sim 18$ cm, hence the bulk scattering is not diminished by absorption effects.
[31]G. S. Higashi, Y. J. Chabal, G. W. Trucks, and K. Raghavachari, Appl. Phys. Lett. **56**, 656 (1990).
[32]A general reference supporting this, for solids and liquids, is A. Braslau, P. S. Pershan, G. Swislow, B. M. Ocko, and J. Als-Nielsen, Phys. Rev. A **38**, 2457 (1988).
[33]D. K. Schwartz, M. L. Schlossman, E. H. Kawamoto, G. J. Kellogg, P. S. Pershan, and B. M. Ocko, Phys. Rev. A **41**, 5687 (1990).
[34]M. K. Sanyal, S. K. Sinha, K. G. Huang, and B. M. Ocko, Phys. Rev. Lett. **66**, 628 (1991).
[35]D. F. Brewer, in *The Physics of Liquid and Solid Helium,* edited by K. H. Bennemann and J. B. Ketterson (Wiley, New York, 1977), p. 573.
[36]E. Cheng and M. Cole, Phys. Rev. B **38**, 987 (1988).
[37]E. S. Sabisky and C. H. Anderson, Phys. Rev. A **7**, 790 (1973). The Hamaker constant can be equivalently expressed as 28 K-layers as compared with the theoretical value for pure silicon of 36.3 K-layers. The discrepancy between the measured value and the theoretical prediction is most likely due to relativistic corrections to the van der Waals interaction.
[38]M. W. Cole, M. R. Swift, and F. Toigo, Phys. Rev. Lett. **69**, 2682 (1992).
[39]I. M. Tidswell, T. A. Rabedeau, P. S. Pershan, J. P. Folkers, M. V. Baker, and G. M. Whitesides, Phys. Rev. B **44**, 10869 (1991).
[40]M. O. Robbins, D. Andelman, and J. F. Joanny, Phys. Rev. A **43**, 4344 (1991).
[41]I. M. Tidswell, T. A. Rabedeau, P. S. Pershan, and S. D. Kosowsky, Phys. Rev. Lett. **66**, 2108 (1991).
[42]D. T. Smith and R. B. Hallock, Phys. Rev. B **34**, 226 (1986).
[43]Semiconductor Processing Corp., Boston, MA.
[44]E. Cheng, M. W. Cole, W. F. Saam, and J. Treiner, Phys. Rev. Lett. **67**, 1007 (1991).
[45]J. Treiner (private communication).
[46]L. D. Landau and E. M. Lifshitz, *Fluid Mechanics* (Pergamon, Elmsford, 1987).
[47]A. J. Ikushima, M. Iino, and M. Suzuki, Can. J. Phys. **65**, 1505 (1987).
[48]A. Guirao, M. Centelles, M. Barranco, M. Pi, A. Polls, and X. Vinas, J. Phys. **4**, 667 (1992).
[49]G. K. White, *Experimental Techniques in Low-Temperature Physics,* 3rd ed. (Oxford University Press, Oxford, 1987).
[50]C. F. Mate and S. P. Sawyer, Phys. Rev. Lett. **20**, 834 (1968).
[51]G. L. Pollack, Rev. Mod. Phys. **41**, 48 (1969).
[52]I. M. Khalatnikov, *An Introduction to the Theory of Superfluidity* (Benjamin, New York, 1965).

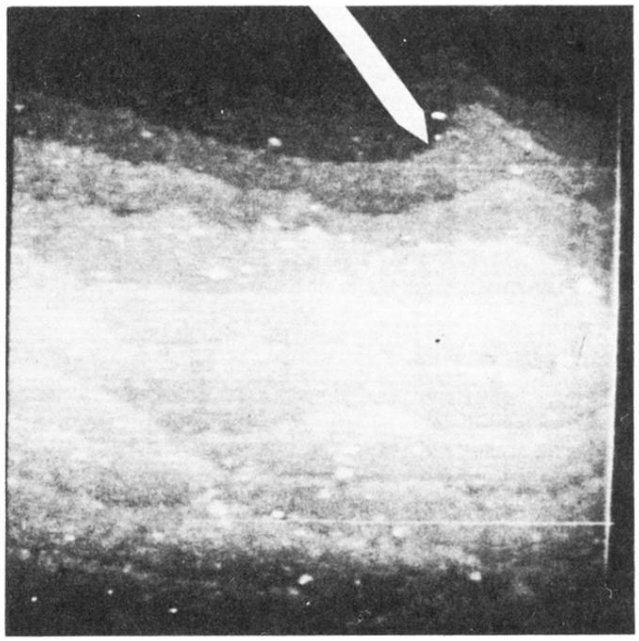

FIG. 7. STM image of hydrogen passivated Si(111) surface. This image was made after removing the substrate from the cryostat and a subsequent brief exposure to air. Although individual atoms are not visible terrace edges due to the crystal miscut can be clearly discerned (arrow).